Available online at www.sciencedirect.com
SCIENCE DIRECT®
Remote Sensing of Environment 86 (2003) 303–321
Remote Sensing of Environment
www.elsevier.com/locate/rse

Evaluating environmental influences of zoning in urban ecosystems with remote sensing

Jeffrey S. Wilson[a,*], Michaun Clay[b,1], Emily Martin[a,2], Denise Stuckey[c,3], Kim Vedder-Risch[d,4]

[a] *Department of Geography, Indiana University-Purdue University, 425 University Boulevard, Indianapolis, IN 46202-5143, USA*
[b] *City of Indianapolis, USA*
[c] *The Schneider Corporation, USA*
[d] *Indiana Department of Environmental Management, USA*

Received 26 March 2002; received in revised form 11 July 2002; accepted 2 March 2003

Abstract

The influence of zoning on Normalized Difference Vegetation Index (NDVI) and radiant surface temperature (T_s) measurements is investigated in the City of Indianapolis, IN, USA using data collected by the Enhanced Thematic Mapper Plus (ETM+) remote sensing system. Analysis of variance indicates statistically significant differences in mean T_s and NDVI values associated with different types of zoning. Multiple comparisons of mean T_s and NDVI values associated with specific pairings of individual zoning categories are also shown to be significantly different. An inverse relationship between T_s and NDVI was observed across the city as a whole and within all but one zoning category. A range of environmental influences on sensible heat flux and urban vegetation was detected both within and between individual zoning categories. Examples for implementing these findings in urban planning applications to find examples of high and low impact development are demonstrated.

Keywords: Zoning; Urban ecosystems; Remote sensing

1. Introduction

Zoning is one of several tools urban planners use to control physical characteristics of developing landscapes by imposing restrictions on variables such as maximum building height and density, extent of impervious surface and open space, and land use types and activities. These variables, in turn, influence environmental processes of atmosphere/surface energy exchange (Grimmond & Oke, 1995; Quattrochi & Ridd, 1994), surface and subsurface hydrologic systems (Grimmond & Oke, 1991; Hammer, 1972), and micro- to mesoscale weather and climate regimes (Changnon, 1992; Oke, 1987; Roth, Oke, & Emery, 1989). The intrinsic relationships between zoning and the physical structure of urban environments suggest that mechanisms should be in place through which planners can evaluate the environmental consequences of existing zoning ordinances and improve the scientific basis of future decision making in order to mitigate negative effects of development in urban ecosystems. Remote sensing science and technology offers the potential to contribute to this informed decision-making process by providing synoptic data collection capabilities and analysis techniques that generate pertinent information about environmental implications of planning decisions.

The purpose of the research presented in this paper is to contribute to further validation of the applicability of relatively low cost, moderate spatial resolution satellite imagery in urban planning applications and provide some examples of how these data can be used by planners to aid in evaluating environmental impacts of zoning. First, the question of whether or not physical manifestations of

* Corresponding author. Fax: +1-317-274-2347.
E-mail addresses: jeswilso@iupui.edu (J.S. Wilson), c1238@indygov.org (M. Clay), eskempf@iupui.edu (E. Martin), dstuckey@theschneidercorp.com (D. Stuckey), kvedder@dem.state.in.us (K. Vedder-Risch).
[1] Fax: +1-317-327-3192.
[2] Fax: +1-317-274-2347.
[3] Fax: +1-317-826-7200.
[4] Fax: +1-317-232-8714.

0034-4257/03/$ - see front matter © 2003 Elsevier Science Inc. All rights reserved.
doi:10.1016/S0034-4257(03)00084-1

different types of zoning can be differentiated using two objective measurements collected by a satellite remote sensing system is examined. The two measurements examined are radiant surface temperature (T_s) and the Normalized Difference Vegetation Index (NDVI). Second, an analysis of relationships between T_s and NDVI for the entire city and within different zoning categories is presented. Finally, it is shown that zoning results in a range of environmental influences on sensible heat flux and urban vegetation (both within and between different zoning categories). Examples of how these results can be used by urban planners to find instances of high and low impact implementations of different types of zoning are then presented. In the current research, zoning instances with high environmental impact are assumed to be those with reduced vegetation biomass (low NDVI) and/or greater sensible heat flux (high T_s) as compared to other areas that fall within the same zoning category.

It is important to point out that zoning ordinances, while regulatory in nature, are only a guide for development of a landscape. An individual zoning polygon, for example, may contain nonconforming land uses and variances from the characteristics prescribed by a specific zoning ordinance, if it has been developed at all. While there may be a strong correlation between zoning, land use, and land cover, that relationship is governed, in part, by the specific ordinances for that zoning category and how rigorously the ordinances are applied. The intention of this paper is not to reiterate the well-established fact that land use and land cover can have a significant impact on measurements collected by a satellite remote sensing system, but rather to show how remote sensing technology can be used by planners to obtain objective measurements of environmental consequences of existing zoning policies. By examining the spatial variation of T_s and NDVI as a function of zoning, this research demonstrates how planners can construct a comparative context in which to evaluate the implications of existing zoning policies and potentially shape future strategies that lessen the negative impacts of development.

Consider, as a hypothetical example, two different portions of landscape that have both been developed as high-density residential and assume that both of these areas conform to existing zoning ordinances. A planner concerned with environmental consequences of development might ask the questions, ‘‘does one of these areas have a less detrimental impact on the physical environment than the other?’’, ‘‘If so, what are the reasons for these differences and can we use this information to modify existing policies to decrease the environmental consequences of future development?’’. The research presented in this paper seeks to provide a quantitative basis for developing such a comparative context. The City of Indianapolis, IN, USA is used as a case study, but the data and techniques presented should be available and applicable in many moderate- to large-size cities in temperate and tropical climates.

2. Background

Urban planning departments commonly use remote sensing imagery in the development of geographic information system (GIS) databases. For example, vector digitizing from aerial photography has become a common method used in the creation and updating of maps depicting the spatial distribution of basic planning variables such as transportation networks, cadastre, buildings and pavement, land use, and utility infrastructures. The current and coming generations of high spatial resolution earth observation satellites, such as IKONOS and QuickBird, offer the potential for application of spaceborne remote sensing data to some planning applications that were previously limited to aerial photography (Barr & Barnsley, 2000; Jensen & Cowen, 1999). However, while commonly used in certain capacities, the full potential of remote sensing data, particularly quantitative analysis of electromagnetic energy measurements, has not been widely exploited by the planning community (Nichol, 1996; Ryznar & Wagner, 2001) despite the fact that such applications have been suggested at least since the 1960s and 1970s (e.g., Carlson, Augustine, & Boland, 1977; Estes, 1966; Pease, Lewin, & Outcalt, 1976; Wellar & Estes, 1968) and have the potential to improve the quality of planning processes.

As the world’s cities continue to grow in both population and physical size, greater consideration of the manner in which rural lands are developed for urban and suburban land use will become progressively more important (Vitousek, Mooney, Lubchenco, & Melillo, 1997). Planners are increasingly pressured with the challenge of balancing the demands for urban and suburban growth while mitigating the negative environmental impacts of development. Removal of rural land cover types such as soil, water, and vegetation and their replacement with common urban materials such as asphalt, concrete, and metal have significant environmental implications including reduction in evapotranspiration, promotion of more rapid surface runoff, increased storage and transfer of sensible heat, and reduction of air and water quality (Carlson, Dodd, Benjamin, & Cooper, 1981; Goward, 1981; Owen, Carlson, & Gillies, 1998). These changes, in turn, can have negative effects on landscape aesthetics, energy efficiency, human health, and quality of living in urban environments (McPherson et al., 1997; Rosenfeld et al., 1995).

Among the most widely studied consequences of converting rural land cover to urban and suburban development is the urban heat island (UHI), which is manifested by higher surface and air temperatures within urban environments as compared to surrounding rural areas. Approaches to measuring the UHI include sampling of air and surface kinetic temperature at fixed locations, mobile sampling of kinetic temperature from ground and airborne vehicles, and remote measurement of radiant temperature from airborne and spaceborne platforms (Henry, Dicks, Wetterquist, & Roguski, 1989; Stone & Rodgers, 2001). Compromises are

associated with each of these methods, as they measure different aspects of the thermal characteristics of cities (Henry et al., 1989), but remote sensing offers the most synoptic capabilities, at least for measurement of radiant temperature, because of the ability to collect many samples over a broad area almost instantaneously (Saaroni, Ben-Dor, Bitan, & Potcher, 2000). While remote sensing is not a panacea for analysis of urban thermal environments since it only *directly* measures radiant temperature (T_s) from surfaces exposed to the sensors view (Voogt & Oke, 1997, 1998), it can still be a useful tool for gaining an overview of thermal variations within an urban ecosystem. Direct measurements of T_s can also be used in the derivation of hybrid variables such as fractional vegetation cover, impervious surface area, and kinetic surface temperature (Carlson & Arthur, 2000; Carlson, Gillies, & Perry, 1994; Henry et al., 1989; Ji & Jensen, 1999; Nemain, Pierce, Running, & Goward, 1993). Measurements of T_s from the Enhanced Thematic Mapper Plus (ETM+) sensor onboard the recently launched (1999) Landsat 7 satellite are used in the current research because this instrument collects the highest spatial resolution thermal measurements currently available for virtually all of earth's urban areas on a temporally consistent basis.

Vegetation is another important component of the urban ecosystem that has been the subject of much basic and applied research. Urban vegetation influences the physical environment of cities through selective absorption and reflection of incident radiation and regulation of latent and sensible heat exchange (Carlson et al., 1994; Gillies, Cui, Carlson, Kustas, & Humes, 1997; Goward, Cruikhanks, & Hopes, 1985). Commonly cited benefits of urban vegetation include aesthetic enhancement, reduction of air and water pollution (Taha, 1997), increased latent heat exchange (Goward, 1981; Heisler, 1986), increased energy efficiency (Akbari & Taha, 1992; Huang, Akari, Taha, & Rosenfeld, 1987), and contribution to the psychological well-being of urban dwellers (Ulrich, 1986). As in the case of the urban heat island, remote sensing can be a useful tool for studying urban vegetation. In addition to providing measurements of radiant surface temperature, remote sensing instruments collect measurements of reflected energy in the red and near infrared (NIR) portions of the electromagnetic spectrum that can be used to quantify the extent and changing conditions of urban vegetation.

3. Data

3.1. Satellite imagery

A Landsat 7 ETM+ image acquired on June 6, 2000 under relatively clear atmospheric conditions served as the primary data source for mapping of radiant surface temperature and vegetation in the Indianapolis urban ecosystem and as a basis for analysis of the relationship between these variables and zoning categories. The ETM+ sensor is an imaging radiometer that collects measurements of reflected and emitted energy from earth surface features in eight regions of the electromagnetic spectrum ranging from visible to thermal infrared at an 8-bit (0–255) level of quantization. The spatial and spectral characteristics of these eight channels or bands are summarized in Table 1.

The Landsat 7 satellite orbits the earth at an altitude of approximately 700 km following a sun-synchronous, near-polar path at an inclination of 98° from the equator. This orbital pattern provides opportunity to collect imagery of urban environments anywhere between 81° north and south latitudes. The temporal resolution of the sensor (the time it takes to acquire repeat imagery of the same region) is 16 days. On the descending (N to S) daytime portion of an orbit, the satellite crosses the equator at approximately 10:00 AM local solar time, with increasingly later local acquisition times north of the equator, and increasingly earlier local acquisition times south of the equator. The Indianapolis image used in this research (centered at about 39.75°N, 86.16°W) was acquired at approximately 11:15 AM local time (16:15 GMT).

Since urban air temperatures usually reach their maximum sometime after solar noon and maximum thermal contrast in air temperatures between urban and rural air temperatures often occurs at night (Karl, Diaz, & Kukla, 1988; Oke, 1981), the acquisition time of ETM+ imagery may not be considered the most ideal for analysis of the UHI and related phenomena. However, if one takes the urban temperature anomaly as the difference between surface radiant temperatures in the city vs. that in the countryside, the daytime anomaly is typically greater, at least during the summer time. In the current research, it is demonstrated that measurements of both reflective shortwave radiation (in the form of NDVI) and emitted thermal radiation (T_s) collected by the ETM+ sensor provide sufficient contrast to differentiate between not only urban vs. rural, but between different zoning categories within the urban environment.

Landsat images are spatially indexed by a system of paths and rows known as the World Referencing System (WRS). Path numbers refer to the ground track of the

Table 1
Characteristics of Enhanced Thematic Mapper Plus (ETM+) bands

Band	Spatial resolution (m)	Lower limit (μm)	Upper limit (μm)	Bandwidth (nm)	Bits per pixel
1	28.50	0.45	0.52	70	8
2	28.50	0.53	0.61	80	8
3	28.50	0.63	0.69	60	8
4	28.50	0.78	0.90	120	8
5	28.50	1.55	1.75	200	8
6	57.00	10.40	12.50	2100	8
7	28.50	2.09	2.35	260	8
8	14.25	0.52	0.90	380	8

satellite along each orbit, and row numbers refer to the latitudinal center of an image along a given path. The WRS coordinate for the Indianapolis image used in this research is path 021, row 032. The 185-km-wide continuous strip of imagery collected along a given path is divided into 170-km segments prior to distribution, resulting in total areal coverage of approximately 31,500 km^2 per scene. A GIS polygon was used to create a subset of the June 6, 2000 ETM+ image corresponding to the border of Marion County, IN, which shares a common boundary with the City of Indianapolis. The total area of the image analyzed in the research is approximately 1200 km^2.

3.2. Radiometric enhancement

ETM+ imagery processed by the US Geological Survey's Earth Resource Observation Systems (EROS) Data Center to correct for radiometric and geometric distortions are referred to as a Level 1G product. Digital numbers (DNs) in each band of the Level 1G ETM+ imagery used in this research were converted to physical measurements of at sensor radiance (L_λ) using a formula that accounts for the transformation function used to convert the analog signal received at the sensor to DNs stored in the resulting image pixels (Eq. (1)):

$$L_\lambda = \text{gain} \times \text{DN} + \text{offset} \quad (1)$$

where L_λ = at sensor radiance, gain = slope of the radiance/DN conversion function, DN = digital number of a given pixel, and offset = intercept of the radiance/DN conversion function (Landsat Project Science Office, 2002). Gain and offset values are supplied in metadata accompanying each ETM+ image, and the DN to radiance formula (as with all formulas presented in this paper) can easily be implemented using map algebra functions of a raster-based GIS if specialized image processing software was unavailable in an urban planning department. ERDAS Imagine 8.5™ was used as the primary image processing and GIS tool in the current project.

Radiance values were transformed to unitless planetary reflectance for the reflective ETM+ bands (channels 1–5 and 7) and radiant temperature for the thermal band (channel 6). The Landsat Project Science Office (2002) suggests that a reasonable transformation of radiance to reflectance can be achieved for images acquired under relatively clear atmospheric conditions by accounting for the combined reflectance of the surface and atmosphere (Eq. (2)):

$$\rho_p = (\pi L_\lambda d^2)/(\text{ESUN}_\lambda \cos\theta_s) \quad (2)$$

where ρ_p = unitless planetary reflectance, L_λ = spectral radiance at sensor aperture, d = earth–sun distance in astronomical units, ESUN_λ = mean solar exoatmospheric irradiance, and θ_s = solar zenith angle in degrees. Radiance values from the ETM+ thermal band were transformed to radiant surface temperature values using thermal calibration constants supplied by the Landsat Project Science Office (2002) (Eq. (3)):

$$T_s = \text{K2}/(\ln(\text{K1}/L_\lambda + 1)) \quad (3)$$

where T_s = radiant surface temperature (K), K2 = calibration constant 2 (1282.71), K1 = calibration constant 1 (666.09), and L_λ = spectral radiance of thermal band pixels.

Reflectance values from the red (ρ_{red}) and NIR (ρ_{nir}) ETM+ channels were used to compute Normalized Difference Vegetation Index (NDVI) values for the Indianapolis image subset using the formula NDVI=$(\rho_{nir} - \rho_{red})/(\rho_{nir} + \rho_{red})$. The NDVI is a quantitative index useful for monitoring spatial and temporal vegetation dynamics (e.g., Fung & Siu, 2000; Schmidt & Gitelson, 2000; Verstrate & Pinty, 1996). NDVI measures vegetation vigor as a function of spectral reflectance attributed to chloroplast and mesophyll cells in plants and has been shown to have significant relationships with a variety of biophysical properties of vegetation including leaf area index (LAI) (Qi, Moran, Cabot, & Dedieu, 1995), fraction of vegetation ground cover and green biomass (Gamon et al., 1995; Gamon, Field, Roberts, Ustin, & Valentini, 1993), and photosynthetic activity (Reed et al., 1994).

3.3. Geometric correction

NDVI and T_s images of the Indianapolis study region were georeferenced to the Universal Transverse Mercator coordinate system, Zone 16 North in order to facilitate integration of these data with GIS data of the study region. Georeferencing was accomplished using 26 ground control points drawn from 1:24,000 topographic maps, a nearest neighbor resampling algorithm, with a maximum root mean square error (RMSE) of 0.5 pixels. Spatial resolution of the reflective bands was resampled to 30 m and spatial resolution of the thermal band to 60 m in the georeferencing process. Spatial transformations were implemented in such a way that extent of a pixel in the 60-m resolution thermal channel matched exactly the extent of four corresponding 30-m pixels in the reflective bands. This later point was important because subsequent analysis of relationships between T_s and NDVI was achieved by computing the mean NDVI of four pixels and pairing that measurement with the single spatially corresponding value of T_s.

3.4. Geographic information system data

Additional spatial data sources used in the analysis of the Indianapolis urban ecosystem included a GIS polygon layer depicting the spatial distribution of zoning categories within the city, a polygon layer depicting the digitized footprints (plan view) of all structures greater than 10 m^2, and a polygon coverage which delineated the extent of roads. The building footprints and roads GIS layers were created by the City of Indianapolis using on-screen digitizing from

high-resolution (< 0.5 m) aerial photography. These data are employed later in Section 4 of this paper to show how density of development can be integrated with T_s and NDVI to find comparative examples of high and low impact zoning.

The zoning GIS layer was obtained from the Indianapolis Mapping and Geographic Information System (IMAGIS) database and reflected zoning ordinances in place at the time the ETM+ image was acquired. The zoning layer contained 6246 polygons categorized into 77 different zoning categories. Zoning categories were aggregated to two different levels of thematic detail: 13 general zoning categories and 16 detailed categories within the "dwellings" (residential) zoning category (Table 2a and b). The "Dwelling Agricultural" (DA) zoning category was not included in our analysis of the detailed dwellings categorizations because of the heterogeneity of land cover types that occurred within these comparatively large polygons; this category was instead treated as an individual class in the general zoning categorization. Spatial distributions of these zoning categories are depicted in Fig. 1a and b.

Table 2

(a) Residential zoning categories

Residential zoning	Typical density (units/acre)	Primary use	Minimum open space	Typical lot size	Comprehensive plan classification	Number of polygons	% Total city area
DA*	>0.5	agriculture and single-family	85%	3 acres	very low density	699	21.92
DP	varies	planned unit development	varies	varies	varies	89	3.53
DS	0.5	suburban single-family	85%	1 acre	very low density	67	2.22
D1	0.9	suburban single-family	80%	24,000 ft^2	very low density	104	2.16
D2	1.9	suburban single-family	75%	15,000 ft^2	very low density	226	7.16
D3	2.6	low or medium intensity single-family	70%	10,000 ft^2	low density	296	8.53
D4	4.2	low or medium intensity single-family	65%	7200 ft^2	low density	195	4.98
D5	4.5	medium intensity single-family	65%	5000 ft^2	low and medium density	231	8.83
D5II	5.0	medium intensity single- or two-family	65%	3200 ft^2	low and medium density	17	0.13
D6	6–9	low intensity multifamily	(OSR) 3.85	varies	medium density	81	0.83
D6II	9–12	medium intensity multifamily	(OSR) 2.65	varies	medium density	118	1.47
D7	12–15	medium intensity multifamily	(OSR) 2.10	varies	medium density	153	1.40
D8	5–26	urban multi-use residential	(OSR) 2.65	varies	high density	112	0.78
D9	12–120	suburban high-rise apartment	(OSR) 0.29–1.45	varies	high density	29	0.15
D10	20–140	central and inner-city high-rise apartment	(OSR) 0.27–1.18	varies	high density	9	0.02
D11	6.0	mobile dwellings	varies	varies	medium density	23	0.42
D12	5.0	low-density two-family	65%	9000 ft^2	low density	13	0.04

(b) General zoning categories

General zoning	Basic description	Number of polygons	% Total city area
Airport	public airports municipally owned or operated, including all necessary navigation and flight operation facilities, and accessory uses	3	1.39
CBD	central business district—core activities of all types with a variety of related land uses	22	0.30
Commercial	includes office-buffer, high-intensity office/apartment, neighborhood commercial, thoroughfare service, and corridor commercial districts	2013	8.14
Dwellings	variety of residential categories summarized in table above (note: DA treated as separate general zoning class in subsequent analysis)	1763	64.57
Historic	historic preservation district including a variety of land uses (mostly residential)	1	0.01
Hospital	major hospital complexes and campuses	29	0.48
Industrial	variety of industrial uses including urban and suburban and light, medium, and heavy industry	471	9.86
Interstate	interstate highway	4	1.94
Park	permits all sizes and ranges of public park land and facilities, includes park peripheral areas assuring compatibility of adjacent land use	164	4.76
Regional	regional attractions close to CBD including museums, visitor centers, and Indianapolis Zoo	1	0.09
Special use	wide variety of uses such as schools, utility infrastructure, cemeteries, libraries, community centers, charitable organizations, golf courses, and penal institutions	1065	8.12
University	variety of land uses typical of higher education institutions including classroom, office, dormitory, facility maintenance, and parking structures	11	0.36

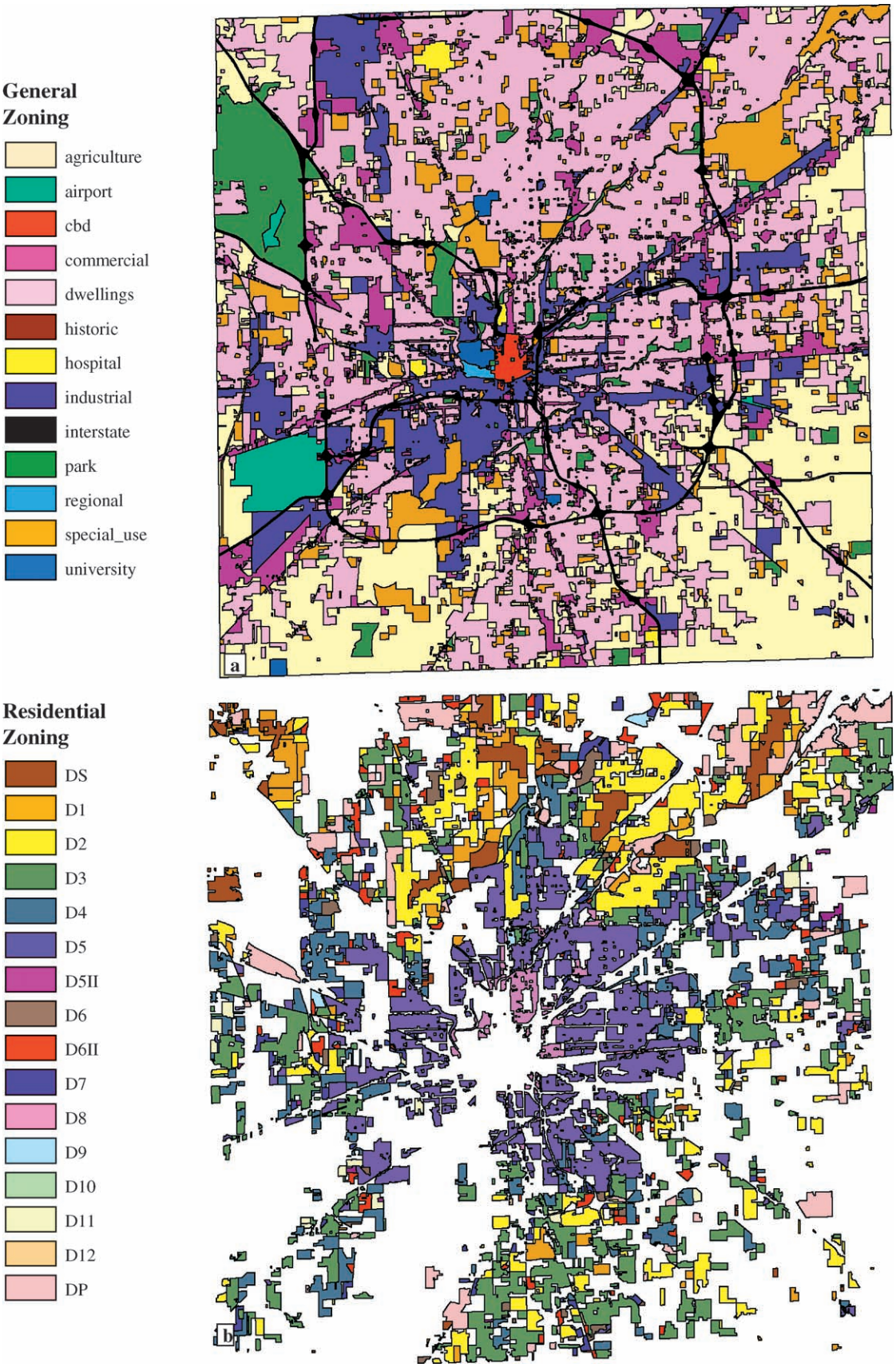

Fig. 1. Map of (a) general zoning categories (b) and detailed residential zoning categories.

4. Analysis

4.1. Visual interpretation of NDVI and T_s imagery

Fig. 2a and b shows the transformed ETM+ data depicting the spatial distribution of NDVI and T_s in the study region. When printed at appropriate scales, such maps provide an informative visual depiction of the spatial distribution of radiant surface temperature and vegetation components within a city, potentially applicable in planning and public education contexts (Fig. 2). In the NDVI image of Indianapolis, the relatively large Eagle Creek and Geist Reservoirs, located in the northwestern and northeastern portion of the county, respectively, appear in dark tones due to the absence of vegetation. Conversely, forested areas around the reservoirs appear in bright tones as a function of relatively high levels of green biomass. The central business district (roughly in the center of image) appears in dark tones, as do some of the commercial and industrial features such as the Indianapolis International Airport (WSW of the CBD near the western edge of the county) and the Indianapolis Motor Speedway (3 km WNW of CBD). Many of the agricultural fields in the study region were only recently plowed or planted by the June 6 image acquisition date so significant crop cover did not have time to develop. These agricultural areas appear in relatively dark gray tones with square or rectangular geometric shapes, particularly in the southeast and southwest corners of the study region. Among the most prominent features in the T_s image of Indianapolis are the bright tones (warmer radiant temperatures) associated with the central portion of the city, some of the major transportation arteries, and adjacent commercial and industrial areas. Cooler radiant surface temperatures (dark tones) are indicated for the reservoirs and surrounding forested areas as well as the White River and adjacent riparian vegetation, which run north to south through the central portion of the city near the center of the image.

4.2. Significance of differences in mean T_s and NDVI by zoning categories

A zonal summary GIS operation was used to derive measurements of central tendency and dispersion of T_s and NDVI associated with different types of zoning at both the general and detailed residential levels of thematic detail. The purpose of creating these statistical summaries was to

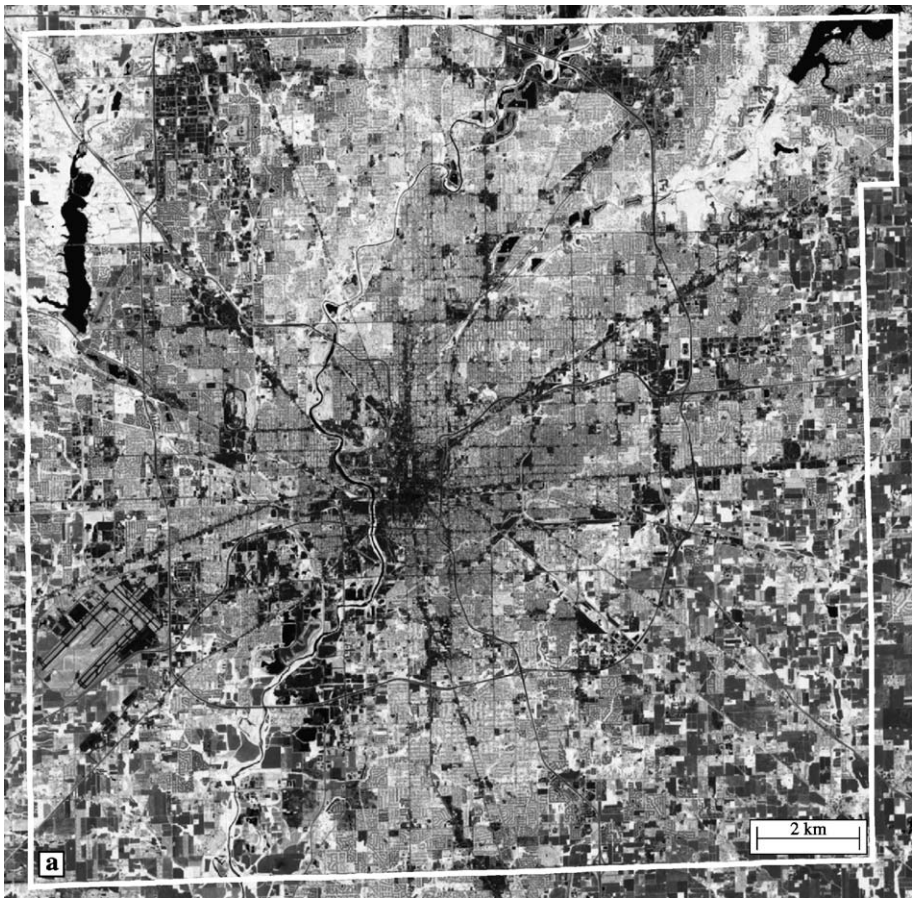

Fig. 2. (a) Normalized difference vegetation index (NDVI) and (b) radiant surface temperature (T_s) images of study region. White line represents extent of Marion County/City of Indianapolis.

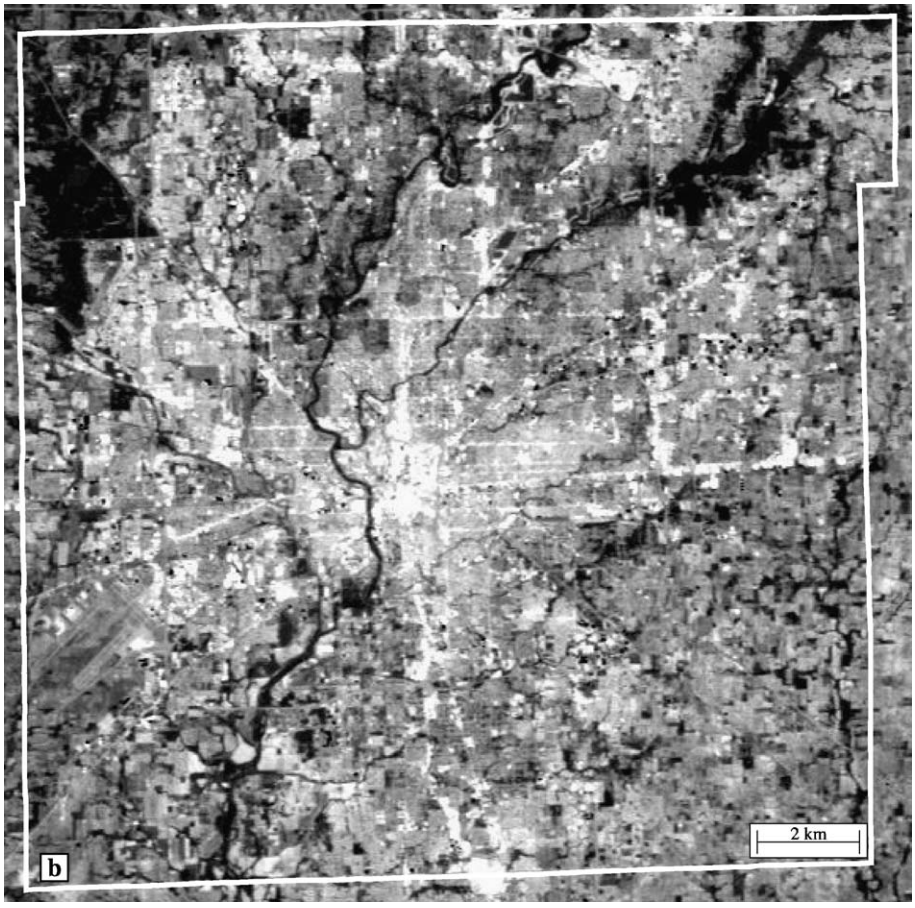

Fig. 2 (*continued*).

provide a database that could be used to address the following research questions.

- How do mean T_s and NDVI values vary between zoning categories and are these variations statistically significant?
- What is the general relationship between NDVI and T_s values in the study region and how does this relationship change within and between different zoning categories?
- How can mean T_s and NDVI values associated with zoning polygons be used by urban planners to evaluate environmental implications of past planning decisions and improve the basis of future decision making?

Fig. 3a and b depicts mean T_s and NDVI values associated with general zoning categories with error bars representing ± 1 standard deviation from the mean. As might be expected, the parks zoning category exhibited the highest mean NDVI value because of the predominance of trees and other vegetated land cover. Greater vegetation cover in the park zoning class suggests comparatively higher rates of evapotranspiration and favoring of latent over sensible heat exchange between surface and atmosphere as compared to more developed locations. This general observation is supported by comparing Fig. 3a and b, where the parks category displays the lowest mean T_s and highest mean NDVI values. The CBD zoning category mirrors the response of parks, having the lowest mean NDVI and highest mean T_s values of the general zoning categories. This observation is indicative of the lack of vegetation and greater sensible heat exchange in the CBD, which forms one of the bases of the UHI effect (Oke, 1982).

Comparable graphs of mean T_s and NDVI values associated with detailed residential zoning categories are provided in Fig. 4a and b. Like the parks category in the general classification, the dwelling suburban (DS) residential zoning category exhibited the lowest mean T_s and highest mean NDVI. The DS category has the lowest housing unit density of the residential zoning categories exclusive to single-family dwellings, and is intended for use "in areas conducive to estate development... or where it is desirable to permit only low density development such as adjacent to flood plains, aquifers, and urban conservation areas" (Metropolitan Development Commission, 1998). Higher mean T_s values were associated with residential zoning categories situated close to the CBD such as the D8 and D5 categories, as well as the D7 category, which is closely associated with commercial shopping centers, industrial areas, and primary transportation arteries.

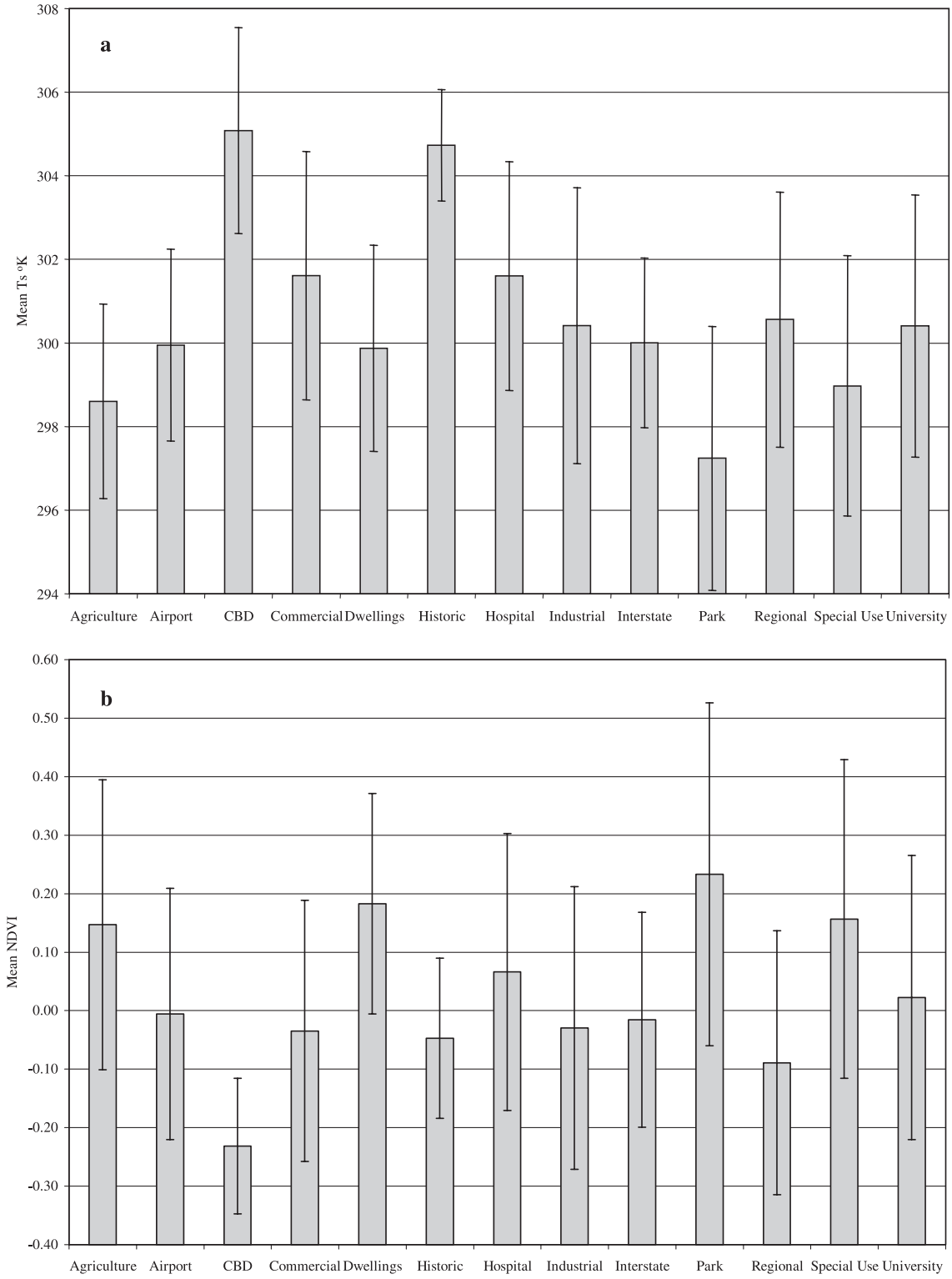

Fig. 3. Mean values of (a) T_s and (b) NDVI associated with general zoning categories.

The applicability of moderate spatial resolution measurements of T_s and NDVI in urban planning depends partly on the ability to use these measurements as a basis for differentiating among different types of land use and land cover of interest to planners. While the error bars presented in Figs. 3 and 4 indicate overlap which occurs between most of the zoning categories for both T_s and NDVI, we were interested in determining whether or not different zoning ordinances have, on average, a significantly different effect on these variables. One-way analysis of variance (ANOVA)

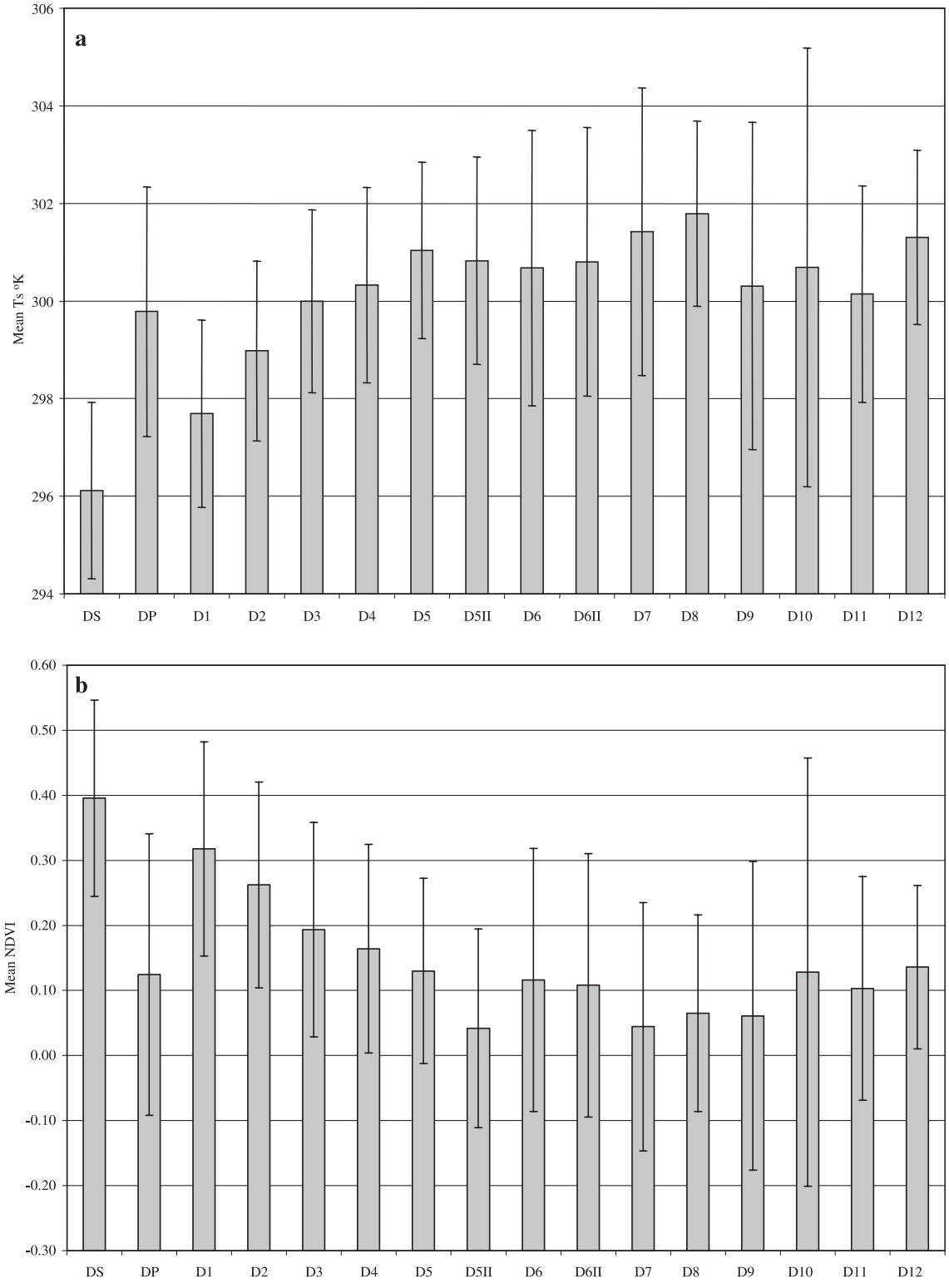

Fig. 4. Mean values of (a) T_s and (b) NDVI associated with residential zoning categories.

tests were used to evaluate the statistical significance of differences in mean T_s and NDVI values associated with different zoning types at the two levels of thematic detail (general zoning and detailed residential zoning). Results of ANOVA tests in all four cases [(1) T_s of general zoning categories, (2) NDVI of general zoning categories, (3) T_s of residential zoning categories, and (4) NDVI of residential zoning categories] indicated that the between groups var-

iance component warranted a rejection of the null hypothesis that there is no significant difference between group means, and acceptance of the alternative hypothesis that mean radiant surface temperature and NDVI are significantly different. The implications of these results suggest that on average, the physical manifestations of different types of zoning have significantly different influences on radiant temperature and vegetation as measured by the ETM+ sensor.

4.3. Multiple comparisons of means

While the ANOVA results indicate that at least some mean T_s and NDVI values are significantly different among the possible pairings of zoning categories, these results do not provide information on which specific pairing(s) differ. To gain further insight, a series of post-hoc multiple comparison tests using Tamhane's T2 were conducted to evaluate the significance of differences in mean T_s and NDVI measurements associated with each possible pairing of zoning categories at both the general and detailed residential levels. Tamhane's T2 post-hoc tests are similar to the Student's *t*-test, but decrease the chance of Type I error for multiple tests by adjusting α as a function of sample size and the number of tests completed. These tests are appropriate in situations where the variance and/or sample size of groups is unequal (Hochberg & Tamhane, 1987). Table 3a and b shows results of post-hoc tests associated with bivariate combinations of general zoning categories for mean T_s and NDVI, respectively. Values in bold italic type indicate cases where the mean difference exceeded the critical value at $\alpha = 0.0001$, indicating a statistically significant difference in mean values associated with a given pairing.

Of the 78 possible combinations of general zoning categories, 66 pairings exhibited significantly different mean values of T_s. Seventy-three pairings were significantly different in terms of mean NDVI. For example, mean T_s of the agriculture zoning class was significantly different from all other general zoning classes, while pairings such as CBD and historic, and commercial and hospital were not significantly different. Similarly, mean NDVI associated with the historic zoning was not significantly different from industrial, regional, and interstate zoning, while agriculture, CBD, and dwelling categories were significantly different from all other general zoning categories. The same multiple comparison procedures were used to test for significant differences in mean T_s and NDVI values associated with detailed residential zoning categories (Table 4a and b). Of the 120 possible combinations of detailed residential zoning classes, 83 pairings displayed significantly different mean values of T_s.

Table 3
Results of post-hoc tests to evaluate significance of differences in (a) mean T_s and (b) mean NDVI values associated with bivariate combinations of general zoning categories

	Agriculture	Airport	CBD	Commercial	Dwellings	Historic	Hospital	Industrial	Interstate	Park	Regional	Special use
(a) Tamhane's T2 multiple comparison table of mean differences in T_s for general zoning categories												
Airport	***−1.34***											
CBD	***−6.48***	***−5.14***										
Commercial	***−3.00***	***−1.66***	***3.48***									
Dwellings	***−1.27***	0.08	***5.21***	***1.74***								
Historic	***−6.12***	***−4.78***	0.36	***−3.12***	***−4.86***							
Hospital	***−3.00***	***−1.66***	***3.48***	0.01	***−1.73***	***3.13***						
Industrial	***−1.81***	***−0.47***	***4.67***	***1.19***	***−0.54***	***4.31***	***1.19***					
Interstate	***−1.40***	−0.06	***5.08***	***1.60***	***−0.13***	***4.72***	***1.60***	***0.41***				
Park	***1.37***	***2.71***	***7.85***	***4.37***	***2.63***	***7.49***	***4.36***	***3.17***	***2.77***			
Regional	***−1.95***	−0.61	***4.53***	***1.05***	−0.69	***4.17***	***1.05***	−0.14	−0.55	***−3.32***		
Special use	***−0.37***	***0.97***	***6.11***	***2.63***	***0.90***	***5.75***	***2.63***	***1.44***	***1.03***	***−1.73***	***1.58***	
University	***−1.80***	−0.45	***4.68***	***1.21***	***−0.53***	***4.33***	***1.20***	0.01	−0.40	***−3.16***	0.16	***−1.43***
(b) Tamhane's T2 multiple comparison table of mean differences in NDVI for general zoning categories												
Airport	***0.15***											
CBD	***0.38***	***0.23***										
Commercial	***0.18***	***0.03***	***−0.20***									
Dwellings	***−0.04***	***−0.19***	***−0.41***	***−0.22***								
Historic	***0.19***	0.04	***−0.18***	0.01	***0.23***							
Hospital	***0.08***	***−0.07***	***−0.30***	***−0.10***	***0.12***	***−0.11***						
Industrial	***0.18***	***0.02***	***−0.20***	***0.00***	***0.21***	−0.02	***0.10***					
Interstate	***0.16***	***0.01***	***−0.22***	***−0.02***	***0.20***	−0.03	***0.08***	***−0.01***				
Park	***−0.09***	***−0.24***	***−0.46***	***−0.27***	***−0.05***	***−0.28***	***−0.17***	***−0.26***	***−0.25***			
Regional	***0.24***	***0.08***	***−0.14***	***0.05***	***0.27***	0.04	***0.16***	***0.06***	***0.07***	***0.32***		
Special use	***−0.01***	***−0.16***	***−0.39***	***−0.19***	***0.03***	***−0.20***	***−0.09***	***−0.19***	***−0.17***	***0.08***	***−0.25***	
University	***0.12***	***−0.03***	***−0.25***	***−0.06***	***0.16***	***−0.07***	***0.04***	***−0.05***	***−0.04***	***0.21***	***−0.11***	***0.13***

Values in bold italic-type indicate pairings where the mean difference exceeded critical value at $\alpha = 0.0001$.

Table 4
Results of post-hoc tests to evaluate significance of differences in (a) mean T_s and (b) mean NDVI values associated with bivariate combinations of residential zoning categories

	DS	DP	D1	D2	D3	D4	D5	D5II	D6	D6II	D7	D8	D9	D10	D11
(a) Tamhane's T2 multiple comparison table of mean differences in T_s for residential zoning categories															
DP	***−3.67***														
D1	***−1.57***	***2.09***													
D2	***−2.86***	***0.81***	***−1.29***												
D3	***−3.88***	***−0.21***	***−2.30***	***−1.02***											
D4	***−4.21***	***−0.54***	***−2.64***	***−1.35***	***−0.33***										
D5	***−4.92***	***−1.26***	***−3.35***	***−2.06***	***−1.04***	***−0.71***									
D5II	***−4.71***	***−1.05***	***−3.14***	***−1.85***	***−0.83***	−0.50	0.21								
D6	***−4.56***	***−0.89***	***−2.99***	***−1.70***	***−0.68***	***−0.35***	***0.36***	0.15							
D6II	***−4.69***	***−1.02***	***−3.11***	***−1.83***	***−0.81***	***−0.47***	***0.24***	0.03	−0.12						
D7	***−5.30***	***−1.64***	***−3.73***	***−2.44***	***−1.43***	***−1.09***	***−0.38***	−0.59	***−0.74***	***−0.62***					
D8	***−5.67***	***−2.01***	***−4.10***	***−2.81***	***−1.79***	***−1.46***	***−0.75***	***−0.96***	***−1.11***	***−0.99***	***−0.37***				
D9	***−4.19***	***−0.52***	***−2.62***	***−1.33***	−0.31	0.02	0.73	0.52	***0.37***	0.50	***1.11***	***1.48***			
D10	***−4.57***	−0.91	−3.00	−1.71	−0.69	−0.36	0.35	0.14	−0.01	***0.11***	0.73	1.10	−0.38		
D11	***−4.03***	−0.36	***−2.45***	***−1.17***	−0.15	0.18	***0.90***	***0.69***	0.53	0.66	***1.28***	***1.65***	0.16	0.55	
D12	***−5.19***	***−21.52***	***−3.62***	***−2.33***	***−1.31***	***−0.98***	−0.27	−0.48	−0.63	−0.50	0.12	0.48	−1.00	−0.62	***−1.16***
(b) Tamhane's T2 multiple comparison table of mean differences in NDVI for residential zoning categories															
DP	***0.27***														
D1	***0.08***	***−0.19***													
D2	***0.13***	***−0.14***	***0.06***												
D3	***0.20***	***−0.07***	***0.12***	***0.07***											
D4	***0.23***	***−0.04***	***0.15***	***0.10***	***0.03***										
D5	***0.27***	−0.01	***0.19***	***0.13***	***0.06***	***0.03***									
D5II	***0.35***	***0.08***	***0.28***	***0.22***	***0.15***	***0.12***	***0.09***								
D6	***0.28***	0.01	***0.20***	***0.15***	***0.08***	***0.05***	***0.01***	***−0.07***							
D6II	***0.29***	***0.02***	***0.21***	***0.15***	***0.09***	***0.06***	***0.02***	***−0.07***	0.01						
D7	***0.35***	***0.08***	***0.27***	***0.22***	***0.15***	***0.12***	***0.09***	0.00	***0.07***	***0.06***					
D8	***0.33***	***0.06***	***0.25***	***0.20***	***0.13***	***0.10***	***0.07***	***−0.02***	***0.05***	***0.04***	***−0.02***				
D9	***0.33***	***0.06***	***0.26***	***0.20***	***0.13***	***0.10***	***0.07***	−0.02	***0.06***	***0.05***	−0.02	0.00			
D10	***0.27***	0.00	***0.19***	***0.13***	0.07	0.04	0.00	−0.09	−0.01	−0.02	−0.08	−0.06	−0.07		
D11	***0.29***	***0.02***	***0.21***	***0.16***	***0.09***	***0.06***	***0.03***	***−0.06***	0.01	0.00	***−0.06***	***−0.04***	***−0.04***	0.03	
D12	***0.26***	−0.01	***0.18***	***0.13***	***0.06***	0.03	−0.01	***−0.09***	−0.02	−0.03	***−0.09***	***−0.07***	***−0.07***	−0.01	***−0.03***

Values in bold italic-type indicate pairings where the mean difference exceeded critical value at $\alpha = 0.0001$.

Ninety-four pairings were significantly different in terms of mean NDVI measurements. Overall, multiple comparisons of means indicated that more zoning categories could be differentiated on the basis of NDVI as compared to T_s at both the general and detailed levels.

4.4. Relationships between T_s and NDVI

A significant inverse relationship between T_s and NDVI has been well documented in the remote sensing literature for both urban and rural environments (e.g., Gallo & Tarpley, 1996; Goward, Xue, & Czajkowski, 2002). The basis of this relationship is that higher levels of latent heat exchange are more typical of areas characterized by significant vegetation cover as compared to areas with little or no vegetation cover and low surface moisture availability, such as densely developed urban areas, where sensible heat exchange is favored (Oke, 1982; Owen et al., 1998). Sobrino and Raissouni (2000), for example, used the inverse relationship between NDVI and radiant surface temperature measurements collected in multitemporal Advanced Very High Resolution Radiometer (AVHRR) imagery for characterizing land cover dynamics in Morocco. Lo, Quattrochi, and Luvall (1997) found significant inverse relationships between NDVI and radiant temperature associated with residential and agricultural land use in suburban areas of Huntsville, AL using high-resolution measurements captured by the airborne Advanced Thermal and Land Applications Sensor (ATLAS). Gallo and Owen (1998) used the inverse relationship between T_s and NDVI for categorizing urban and rural climate monitoring stations as a function of predominate surrounding land cover type. Carlson et al. (1994) and Gillies and Carlson (1995) expanded on the inverse relationship between T_s and NDVI to develop methods for quantifying additional biophysical variables including fractional vegetation cover and soil moisture availability.

The inverse relationship between T_s and NDVI in the Indianapolis urban ecosystem is depicted in Fig. 5, a scatter plot in which the horizontal axis represents NDVI and the vertical axis represents T_s. Each point represents the mean T_s and NDVI value associated with one of the 6462 zoning polygons in the study region. The relationship between these variables was quantified for the entire city and within

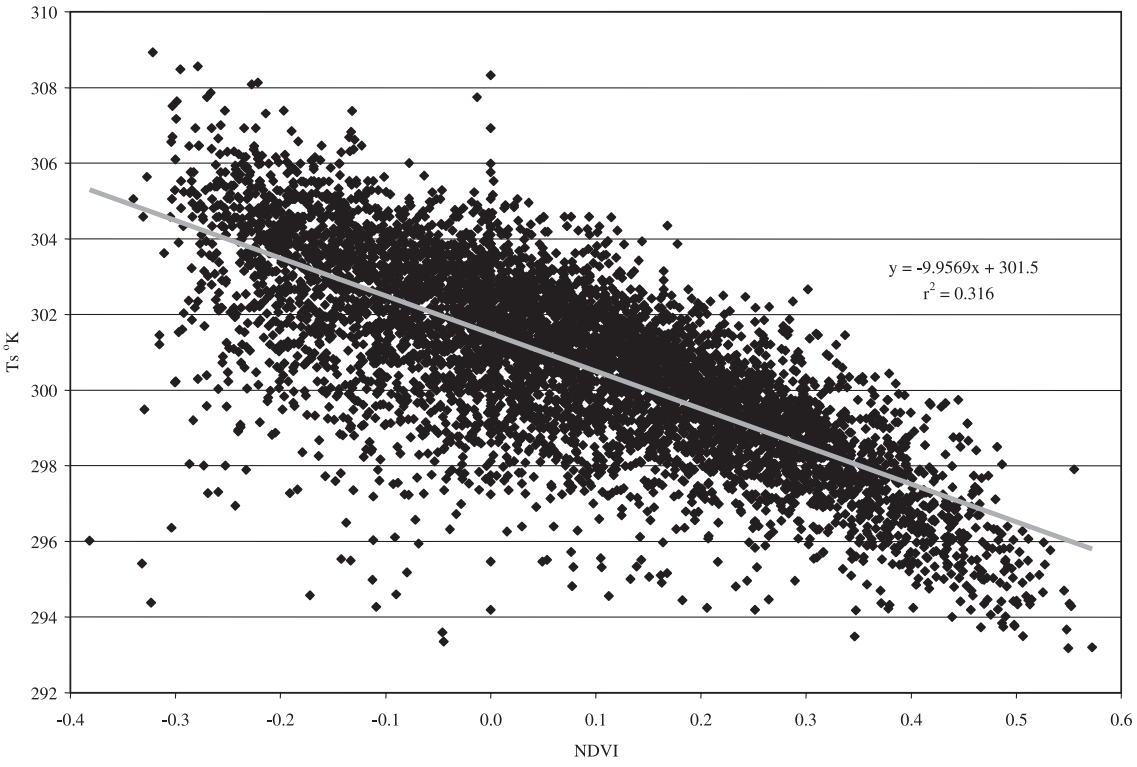

Fig. 5. Scatter plot of mean NDVI (*x*-axis) and T_s (*y*-axis) associated with each zoning polygon in the Indianapolis study region.

each of the general and detailed residential zoning categories by computing a series of Pearson Product Moment Correlation coefficients (Table 5). These tests were developed by analyzing the relationship between each pixel value from the T_s image and the mean of the four corresponding pixels from the NDVI image. Aside from the correlation computed for the entire city, each test included only the pixels delineated in the respective zoning categories as defined by the zoning GIS layer.

Correlation results show that relationships between T_s and NDVI were significant for the city as a whole and within all individual zoning categories except for the regional category in the general zoning classification. At the time the June 6, 2000 ETM+ image was acquired, there was one polygon zoned as regional, which occurred just to the west of the CBD. This area of the city includes regional attractions such as a relatively new baseball stadium (Victory Field), the Indianapolis Zoo, the White River State Park Visitor's Center, and proportionally, a relatively large segment of the White River (Fig. 6a). The low correlation coefficient between T_s and NDVI for this zoning polygon can be attributed to the large area that is occupied by water, which has very low NDVI and also low values of T_s. Similarly, the low but statistically significant relationship between T_s and NDVI for the parks zoning category is primarily a function of the inclusion of Eagle Creek Reservoir in the parks category (Fig. 6b).

It has been well documented in the remote sensing literature that relationship between T_s and NDVI is strongly influenced by the presence of water, both in the form of moisture contained in soil and vegetation, as well as surface water features such as lakes, ponds, and rivers (e.g., Carlson et al., 1981; Gillies & Carlson, 1995). Excluding pixels that correspond to major surface water features from the analysis would undoubtedly increase the significance of the relationship between T_s and NDVI and tighten up the dispersion of points around the regression line depicted in Fig. 5. This would be a desirable modification to the methods presented here if the objective was to study only land surfaces. However, in the context of the current research, surface water pixels were not excluded for several reasons.

First, the sighting of specific types of zoning around the surface water features such as lakes and rivers often represents a conscious decision on the part of planners. Since the intention of this research is to analyze individual zoning polygons as a unit of the urban landscape, excluding water pixels would preclude comparative analysis of specific instances of zoning within their respective environmental contexts. Secondly, surface water in the form of retention ponds located in many of the newer residential developments within the Indianapolis/Marion County study region is a direct result of planning policies to account for increased storm water runoff created by the addition of impervious surfaces and has been a point of debate among planners, developers, and residents. Exclusion of surface water pixels in this case would inhibit the ability of planners to evaluate the effects of different forms of

Table 5
Pearson product moment correlation coefficients and coefficients of determination for the relationship between T_s and NDVI for (a) general zoning classes and (b) residential zoning classes

	r	r^2	sig.
(a) General zoning			
Agriculture	−0.665	0.443	*
Airport	−0.658	0.433	*
CBD	−0.440	0.193	*
Commercial	−0.632	0.400	*
Dwellings	−0.661	0.436	*
Historic	−0.677	0.459	*
Hospital	−0.787	0.619	*
Industrial	−0.484	0.234	*
Interstate	−0.571	0.326	*
Park	−0.268	0.072	*
Regional	−0.009	0.000	
Special use	−0.523	0.274	*
University	−0.669	0.447	*
Entire city	−0.563	0.316	*
(b) Residential zoning			
DS	−0.616	0.380	*
DP	−0.520	0.271	*
D1	−0.523	0.274	*
D2	−0.593	0.351	*
D3	−0.647	0.419	*
D4	−0.649	0.421	*
D5	−0.701	0.491	*
D5II	−0.682	0.465	*
D6	−0.450	0.202	*
D6II	−0.588	0.346	*
D7	−0.361	0.130	*
D8	−0.627	0.394	*
D9	−0.520	0.271	*
D10	−0.913	0.834	*
D11	−0.670	0.449	*
D12	−0.647	0.419	*

Statistical significance at $\alpha = 0.01$ for two-tailed test at corresponding *df* signified by *.

accounting for increased impervious surface area on T_s and NDVI. An additional reason for not excluding pixels that correspond to surface water features relates to the spatial resolution of the imagery. While major surface water features in the study region, such as the larger streams and reservoirs, could be masked out of the 60-m resolution thermal imagery, smaller surface water features would still be included in the form of mixed pixels, in which a measurement for a pixel is a function of both water and land surface that occurs within a pixel instantaneous field of view. There are many mixed water/land surface pixels in the imagery of the Indianapolis study region that result from, for example, smaller retention ponds and streams that occur within developed areas, drainage ditches in agricultural areas, and the Whitewater Canal, which runs through the western portion of the Indianapolis CBD. Thus, at some point, the removal of large surface water features and the inclusion of smaller surface water features in the form of mixed pixels may ultimately bias the results.

4.5. Example applications of T_s and NDVI feature space in urban planning

A potential application of the inverse relationship between T_s and NDVI in urban planning is to use this phenomenon as a comparative tool for finding examples of low and high impact implementations within a particular zoning category. Consider that all polygons making up a particular zoning category provide examples of a range of possible development options. By examining variations of mean T_s and NDVI within this group, planners can find examples of both high impact implementations, in which development has led to low levels of green biomass and/or high levels of radiant temperature (i.e., low NDVI and high T_s), and low impact implementations, where NDVI remains high and/or surface temperatures are relatively low. Below, we use the DP (planned unit development) residential zoning category to illustrate this concept.

Fig. 7 shows a scatter plot of mean T_s and NDVI associated with the 89 DP zoning polygons that occur in the study region. High-resolution (5 m) near infrared aerial imagery is used to illustrate the nature of land use and land cover within selected polygons occurring in different locations of the T_s/NDVI feature space. Points occurring at the lower right of the scatter plot represent examples that could be categorized as low impact implementations, while those at the upper left represent high impact implementations. The image at upper right shows a relatively new and affluent single-family development zoned as DP, which might be categorized as a low impact implementation in terms of effect on T_s and NDVI. This subdivision occurs along the southern portion of Geist Reservoir, and a significant amount of tree cover was left intact during the development. Tree cover appears as middle gray tones located to the rear of individual houses, while grass appears in brighter tones, located primarily in the front of the houses. While the dark area around the development represents the surface water of the reservoir, the lake itself is not part of the same polygon, and thus has no direct effect on the location of this zoning unit in the T_s/NDVI feature space image. The image at upper left represents what might be categorized as a high impact example, displaying high mean T_s and low mean NDVI. This area consists of multifamily apartment buildings, with little vegetation left intact. Mean T_s remains high despite the retention ponds that are included in the center of the polygon, which have an effect of pulling the location of this zoning polygon towards the origin the graph. The image at lower left depicts what might be categorized as an outlier in the sense that while the mean NDVI value is relatively low, so is the mean T_s value. Like the regional and park examples shown in Fig. 6, this polygon exhibits low correlation between T_s and NDVI because of the relatively large proportion covered by water. This development occurs on the site of a former gravel quarry.

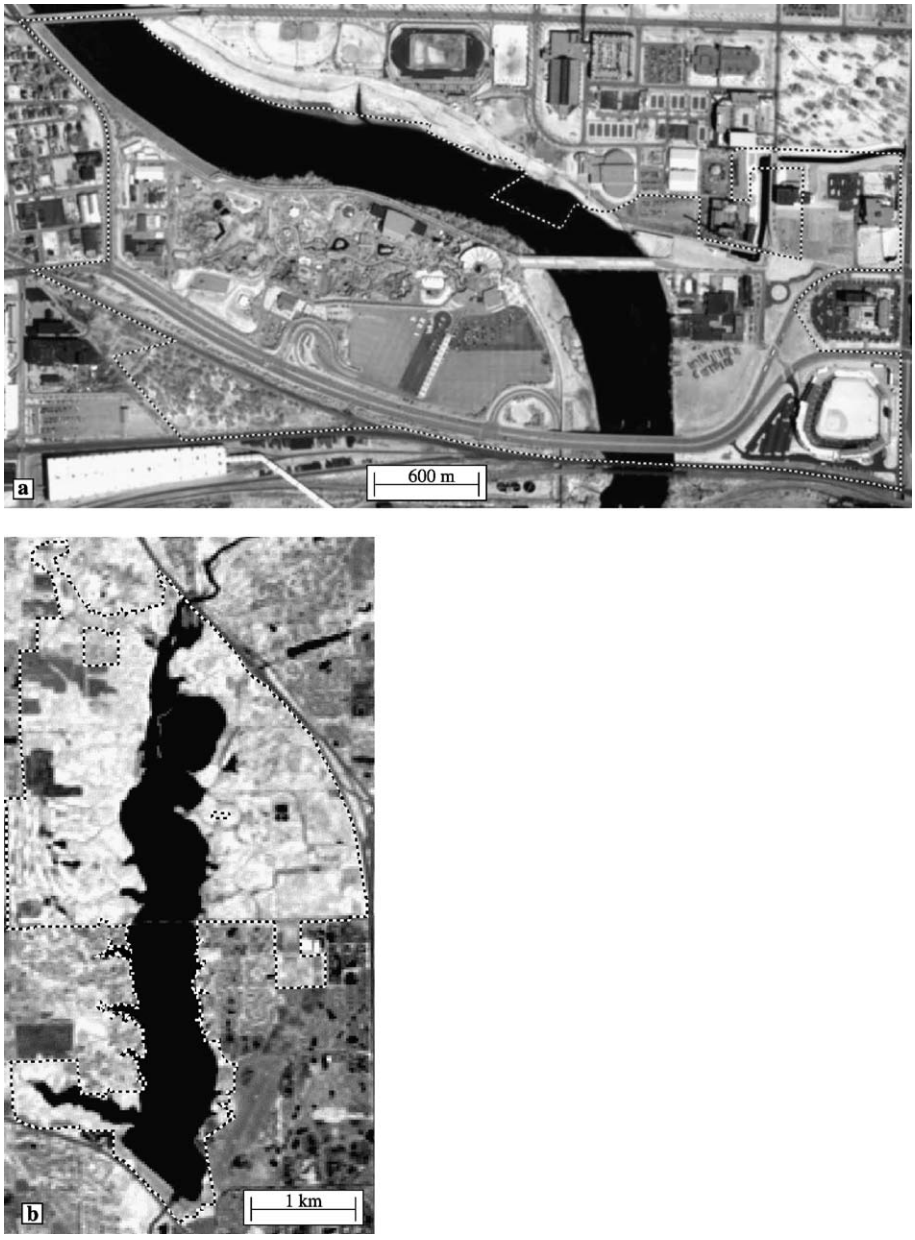

Fig. 6. Examples of zoning polygons exhibiting low correlation between T_s and NDVI: (a) 5-m panchromatic aerial image of regional zoning polygon, (b) 30-m resolution near infrared ETM+ (Band 4) image of Eagle Creek Park Polygon.

4.6. Extending the T_s/NDVI feature space model

A possible point of contention arising from the results presented thus far is that most of the low environmental impact (i.e., high NDVI and/or low T_s) examples of zoning ordinances observed in the study region are characterized by low-density development (e.g., the single family housing development shown in the upper right of Fig. 7 and the DS residential zoning category). These forms of development may be considered the least desirable to planners who cite low-density development as an undesirable trait in the context of urban sprawl. A more compliant application of the comparison of zoning in T_s/NDVI feature space from the perspective of mitigating urban sprawl would be the inclusion of third axis of development density—the idea being that the most ideal examples of development would exhibit some combination of low T_s, high NDVI, and high-density development.

An example of extending the T_s/NDVI feature space by adding a third axis of development density is presented in Fig. 8a. The third axis represents the percent of the zoning polygon covered by developed land cover as defined by building footprint and edge of pavement GIS polygon data. The same DP zoning polygons used in the 2D example above are used here. A zoning polygon that occurs in the "low impact" corner of the 3D feature space is selected to

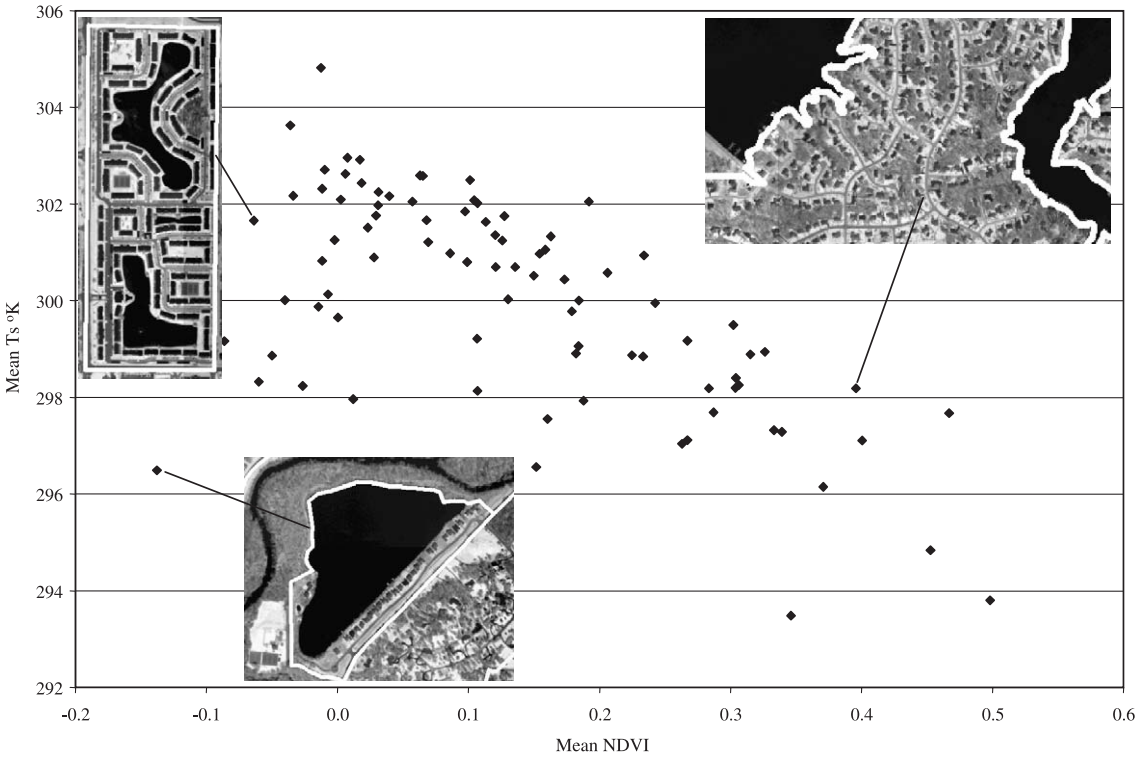

Fig. 7. Scatter plot of mean T_s and NDVI associated with the 89 DP (planned unit development) zoning polygons. Five-meter resolution panchromatic aerial images illustrate land use–land cover of different forms of development within DP ordinance corresponding to selected locations in T_s/NDVI feature space.

illustrate the relationship between what occurs on the ground and how this translates into the feature space graphic. This polygon exhibited a development density value of 37%, a mean NDVI of 0.3, and a mean T_s value of 297°K. This zoning polygon is symbolized by the cube within the 3D feature space graph and contains five multifamily housing structures. Although this zoning unit occurs close to a busy thoroughfare, a fair amount of tree cover has been retained as indicated by the medium gray tones that occur near the edges of the polygon. Instead of creating separate impervious areas to accommodate parking, the developers have included attached garages that also accommodate living space above. The only additional impervious surfaces, aside from the buildings, are the access roads. The remainder of the development is occupied by grass as indicated by the bright tones immediately surrounding the structures.

While graphical comparison of individual zoning units within the 3D feature space provides a visual tool for comparing the impact of landscape units in terms of effect on T_s, NDVI, and development density, this can be extended to a more quantitative index by computing the Euclidean distance from a zoning units location in the 3D feature space to a benchmark location in the "low impact" corner of the graphic. Such an environmental impact index could be computed as (Eq. (4)):

$$\text{Index Value} = \text{SQRT}(X_i - X_j)^2 + (Y_i - Y_j)^2 + (Z_i - Z_j)^2 \quad (4)$$

where X_i, Y_i, and Z_i = the respective values of T_s, NDVI, and development density for a particular zoning unit, and X_j, Y_j, and Z_j = the respective values of T_s, NDVI, and development density for the benchmark location in the low impact portion of feature space. The logic of applying this environmental impact index to the 89 DP zoning polygons in the study region is presented graphically in Fig. 8b. The lines associated with each point represent the Euclidean distance from each DP polygon location in the 3D feature space to the benchmark location. The DP zoning polygon with the lowest index value corresponds to the white cube depicted in Fig. 8a and b. The benchmark value from which Euclidean distance measurements are based in this example was set at $T_s = 295$, NDVI = 0.5, and development density = 65%.

The general idea suggested by these examples is that the integration of city's GIS data with remote sensing measurements of T_s and NDVI provides the opportunity to gain further insight into the environmental consequences of planning decisions. A range of possible development options can be represented in both spatial and quantitative forms, providing a comparative context that relates to the environmental effects imposed by development. This provides planners with the ability to evaluate the effects of existing development and, by exploring the specific reasons for the occurrence of low impact examples, to shape policies that may lessen the impact of future development.

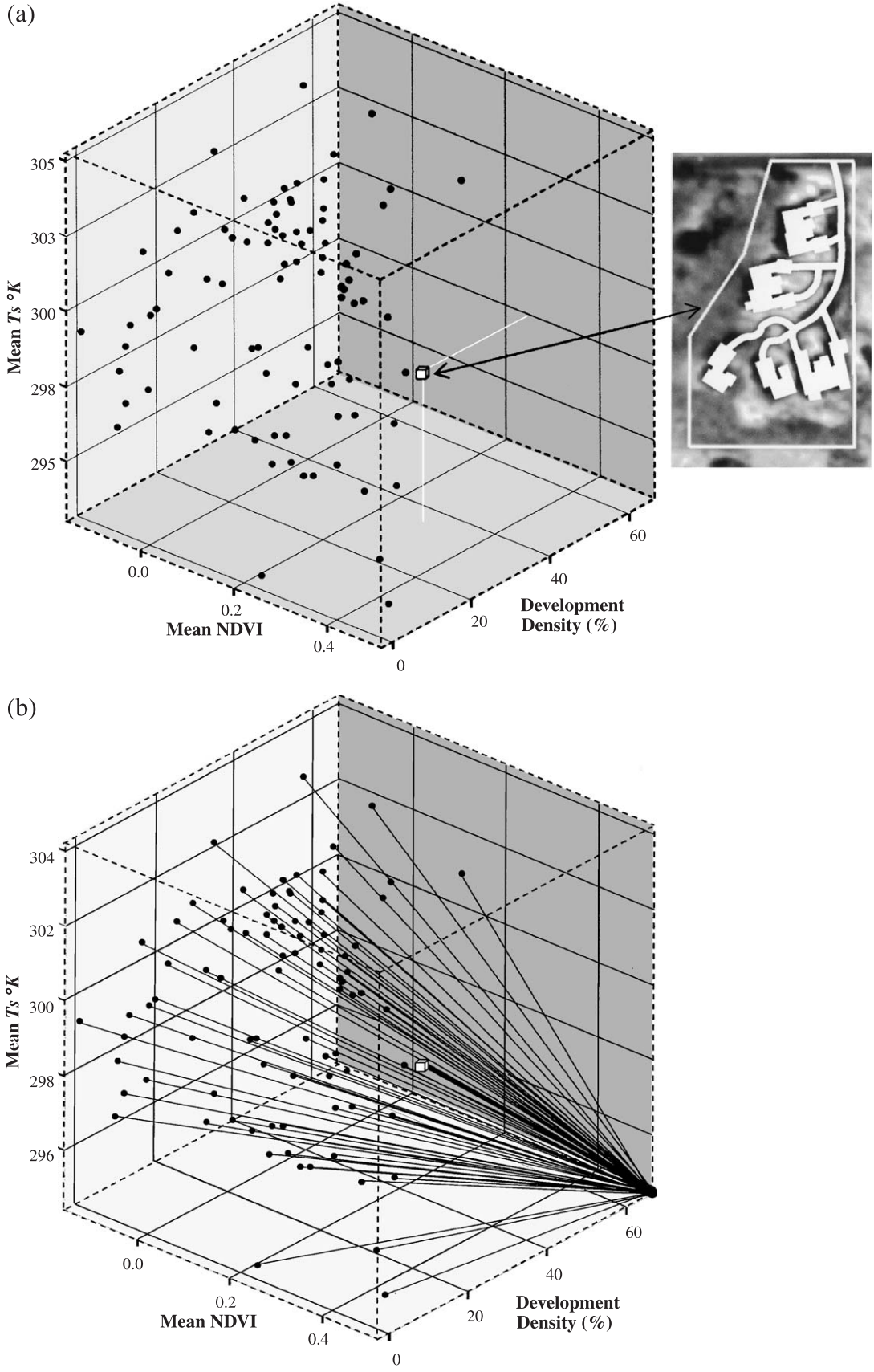

Fig. 8. (a) 3D scatter plot of T_s, NDVI, and % development density associated with the 89 DP (planned unit development) zoning polygons; (b) conceptual diagram of environmental impact index using T_s, NDVI, and % development density.

5. Summary and conclusions

The results of this research indicate that different types of zoning have significantly different effects on radiant surface temperature and NDVI as measured by the ETM+ sensor within the Indianapolis urban ecosystem. Comparisons of mean T_s and NDVI values associated with individual pairings of zoning categories also suggest that the majority can be differentiated on the basis of both T_s and NDVI. A significant inverse relationship between T_s and NDVI was observed for the entire city of Indianapolis and within all but one of the individual zoning categories. Examples of how this relationship can be used by planners to find low and high impact examples within a particular zoning category are provided. An extension of this model that includes the additional variable of development density provides a quantitative index that should be useful to planners that seek examples of development that increase density in the context of slowing urban sprawl, while lessening the impacts of development on radiant temperatures and vegetation.

While zoning polygons were used as the primary unit of analysis in this research, the same methods and concepts could be extended to other forms of urban landscape delineation. Many of the specific decisions that influence radiant surface temperature and vegetation in an urban ecosystem, such as building materials, landscaping, and, to some extent, building form, are often implemented at the development, tract, or individual parcel level (Rosenfeld et al., 1995). This study has shown that moderate spatial resolution remote sensing data, such as that collected by the ETM+ sensor, are useful for regional scale analyses, and the methods presented should be applicable to other forms of urban landscape delineations such as individual developments and neighborhoods. A few examples of the application of higher spatial resolution (e.g., <5 m) multispectral remote sensing imagery for analyzing the impacts of planning on the interactions between radiant temperature and vegetation within urban ecosystems are in development (e.g., Quattrochi et al., 2000; Stone & Rodgers, 2001), but are the exceptions. As higher resolution remote sensing imagery becomes more commonly available, the methods presented in this research could be extended to more specific urban design considerations that impact the thermal and vegetation components of urban ecosystems at finer spatial scales.

Overall, planners have the opportunity to gain significant insight into the physical manifestations of planning policies within cities by integrating quantitative analysis of electromagnetic energy measurements collected by remote sensing systems. Many planning departments already have extensive GIS systems in place that can be adapted to develop analyses such as the one presented in this research. Personnel familiar with principles of map algebra in the raster data model should not have a significant difficulty in extending those skills to analysis of remote sensing imagery. The recent launch of the Landsat 7 satellite equipped with the ETM+ sensor and the control of distribution and pricing of ETM+ imagery by US Federal Government agencies have also had the effect of driving down prices of moderate resolution imagery; ETM+ imagery can currently be purchased for about $600.00 (US) per scene. Thus, with a moderate investment in time and at minimal cost, planners have the potential to add a powerful tool to the planner's toolbox.

References

Akbari, H., & Taha, H. (1992). The impact of trees and white surfaces on residential heating and cooling energy use in four Canadian cities. *Energy*, *17*, 141–149.

Barr, S., & Barnsley, M. (2000). Reducing structural clutter in land cover classifications of high spatial resolution remotely-sensed images for urban land use mapping. *Computers and Geosciences*, *26*, 433–449.

Carlson, T. N., & Arthur, S. T. (2000). The impact of land use–land cover changes due to urbanization on surface microclimate and hydrology: As satellite perspective. *Global and Planetary Change*, *25*, 49–65.

Carlson, T. N., Augustine, J. N., & Boland, F. E. (1977). Potential application of satellite temperature measurements in analysis of land use over urban area. *Bulletin of the American Meteorological Society*, *58*, 1301–1303.

Carlson, T. N., Dodd, J. K., Benjamin, S. G., & Cooper, J. N. (1981). Satellite estimation of the surface energy balance, moisture availability and thermal inertia. *Journal of Applied Meteorology*, *20*, 67–87.

Carlson, T. N., Gillies, R. R., & Perry, E. M. (1994). A method to make use of thermal infrared temperature and NDVI measurement to infer surface soil water content and factional vegetation cover. *Remote Sensing Reviews*, *9*, 161–173.

Changnon, S. A. (1992). Inadvertent weather modification in urban areas: Lessons for global climate change. *Bulletin of the American Meteorological Society*, *73*, 619–627.

Estes, J. E. (1966). Some applications of aerial infrared imagery. *Annals of the Association of American Geographers*, *56*, 673–682.

Fung, T., & Siu, W. (2000). Environmental quality and its changes, and analysis using NDVI. *International Journal of Remote Sensing*, *21*, 1011–1024.

Gallo, K. P., & Owen, T. W. (1998). Assessment of urban heat islands: A multi-sensor approach for the Dallas–Ft. Worth USA region. *Geocarto International*, *13*, 35–41.

Gallo, K. P., & Tarpley, J. D. (1996). The comparison of vegetation index and surface temperature composites of urban heat-island analysis. *International Journal of Remote Sensing*, *17*, 3071–3076.

Gamon, J. A., Field, C. B., Goulden, M., Griffin, K., Hartley, A., Joel, G., Peñuelas, J., & Valentini, R. (1995). Relationships between NDVI, canopy structure, and photosynthetic activity in three Californian vegetation types. *Ecological Applications*, *5*, 28–41.

Gamon, J. A., Field, C. B., Roberts, D. A., Ustin, S. L., & Valentini, R. (1993). Functional patterns in an annual grassland during an AVIRIS overflight. *Remote Sensing of Environment*, *44*, 1–15.

Gillies, R. R., & Carlson, T. N. (1995). Thermal remote sensing of surface soil water content with partial vegetation cover for incorporation into climate models. *Journal of Applied Meteorology*, *34*, 745–756.

Gillies, R. R., Cui, J., Carlson, T. N., Kustas, W. P., & Humes, K. S. (1997). Verification of the 'triangle' method for obtaining surface soil water content and energy fluxes from remote measurements of NDVI and surface radiant temperature. *International Journal of Remote Sensing*, *18*, 3145–3166.

Goward, S. N. (1981). Thermal behavior of urban landscapes and the urban heat island. *Physical Geography*, *2*, 19–33.

Goward, S. N., Cruikhanks, G. D., & Hopes, A. S. (1985). Observed relation between thermal emission and reflected spectral radiance of a complex vegetated landscape. *Remote Sensing of Environment*, *18*, 137–146.

Goward, S. N., Xue, Y., & Czajkowski, K. P. (2002). Evaluating land surface moisture conditions from the remotely sensed temperature/vegetation index measurements: An exploration with the simplified simple biosphere model. *Remote Sensing of Environment*, *79*, 225–242.

Grimmond, C. S. B., & Oke, T. R. (1991). An evapotranspiration–interception model for urban areas. *Water Resources Research*, *27*, 1739–1755.

Grimmond, C. S. B., & Oke, T. R. (1995). Comparison of heat fluxes from summertime observations in the suburbs of four North American cities. *Journal of Applied Meteorology*, *34*, 873–889.

Hammer, T. R. (1972). Stream channel enlargement due to urbanization. *Water Resources Research*, *8*, 1530–1540.

Heisler, G. M. (1986). Energy savings with trees. *Journal of Arboriculture*, *12*, 113–125.

Henry, J. A., Dicks, S. E., Wetterquist, O. E., & Roguski, S. J. (1989). Comparison of satellite, ground-based, and modeling techniques of analyzing the urban heat island. *Photogrammetric Engineering and Remote Sensing*, *55*, 69–76.

Hochberg, Y., & Tamhane, A. (1987). *Multiple comparison procedures*. New York: Wiley. 450 pp.

Huang, J., Akari, H., Taha, H., & Rosenfeld, A. (1987). The potential of vegetation in reducing summer cooling loads in residential buildings. *Journal of Climate and Applied Meteorology*, *26*, 1103–1106.

Jensen, J. R., & Cowen, D. C. (1999). Remote sensing of urban/suburban infrastructure and socio-economic attributes. *Photogrammetric Engineering and Remote Sensing*, *65*, 611–622.

Ji, M., & Jensen, J. R. (1999). Effectiveness of subpixel analysis in detecting and quantifying urban imperviousness from Landsat Thematic Mapper imagery. *Geocarto International*, *14*, 31–39.

Karl, T. R., Diaz, H. F., & Kukla, G. (1988). Urbanization: It detection and effect in the United States climate record. *Journal of Climate and Applied Meteorology*, *1*, 1099–1123.

Landsat Project Science Office (2002). Landsat 7 science data user's handbook. Goddard Space Flight Center. www address: http://ltpwww.gsfc.nasa.gov/IAS/handbook/handbook_toc.html.

Lo, C. P., Quattrochi, D. A., & Luvall, J. C. (1997). Application of high-resolution thermal infrared remote sensing and GIS to assess the urban heat island effect. *International Journal of Remote Sensing*, *18*, 287–304.

McPherson, E. G., Nowak, D., Heisler, G., Grimmond, S., Souch, C., Grant, R., & Rowntree, R. (1997). Quantifying urban forest structure, function, and value: The Chicago Urban Forest Climate Project. *Urban Ecosystems*, *1*, 49–61.

Metropolitan Development Commission (1998). *Dwelling zoning districts for Marion County, Indiana*. Indianapolis: Metropolitan Development Commission. www address: http://www.indygov.org/cp/zonord.htm.

Nemain, R., Pierce, L., Running, S., & Goward, S. (1993). Developing satellite-derived estimates of surface moisture status. *Journal of Applied Meteorology*, *32*, 548–557.

Nichol, J. E. (1996). Analysis of the urban thermal environment with LANDSAT data. *Environment and Planning B: Planning and Design*, *23*, 733–747.

Oke, T. R. (1981). Canyon geometry and the nocturnal urban heat island: Comparison on scale model and field observation. *International Journal of Climatology*, *1*, 237–254.

Oke, T. R. (1982). The energetic basis of the urban heat island. *Quarterly Journal of the Royal Meteorological Society*, *108*, 1–24.

Oke, T. R. (1987). *Boundary layer climates*. New York: Methuen Press. 435 pp.

Owen, T. W., Carlson, T. N., & Gillies, R. R. (1998). An assessment of satellite remotely-sensed land cover parameters in quantitatively describing the climatic effect of urbanization. *International Journal of Remote Sensing*, *19*, 1663–1681.

Pease, R. W., Lewis, J. E., & Outcalt, S. I. (1976). Urban terrain climatology and remote sensing. *Annals of the Association of American Geographers*, *66*, 557–569.

Qi, J., Moran, M. S., Cabot, F., & Dedieu, G. (1995). Normalization of sun/view angle effects using spectral albedo-based vegetation indices. *Remote Sensing of Environment*, *52*, 207–217.

Quattrochi, D. A., Luvall, J. C., Rickman, D. L., Estes Jr., M., Laymon, C. A., & Howell, B. F. (2000). A decision support information system for urban landscape management using thermal infrared data. *Photogrammetric Engineering and Remote Sensing*, *66*, 1195–1207.

Quattrochi, D. A., & Ridd, M. K. (1994). Measurement and analysis of thermal energy responses from discrete urban surfaces using remote sensing data. *International Journal of Remote Sensing*, *15*, 1991–2022.

Reed, B. C., Brown, J. F., VanderZee, D., Loveland, T. R., Merchant, J. W., & Ohlen, D. O. (1994). Measuring phenological variability from satellite imagery. *Journal of Vegetation Science*, *5*, 703–714.

Rosenfeld, A. H., Akbari, H., Bretz, S., Fishman, B. L., Kurn, D. M., Sailro, D., & Taha, H. (1995). Mitigation of urban heat island: Materials, utility programs, updates. *Energy Building*, *22*, 255–265.

Roth, M., Oke, T. R., & Emery, W. J. (1989). Satellite-derived urban heat islands from three coastal cities and the utilization of such data in urban climatology. *International Journal of Remote Sensing*, *10*, 1699–1720.

Ryznar, R. M., & Wagner, T. W. (2001). Using remotely sensed imagery to detect urban change: Viewing Detroit from space. *Journal of the American Planning Association*, *67*, 327–336.

Saaroni, H., Ben-Dor, E., Bitan, A., & Potcher, O. (2000). Spatial distribution and microscale characteristics of the urban heat island in Tel-Aviv, Israel. *Landscape and Urban Planning*, *48*, 1–18.

Schmidt, H., & Gitelson, A. (2000). Temporal and spatial vegetation cover changes in Israeli transition zone: AVHRR-based assessment of rainfall impact. *International Journal of Remote Sensing*, *21*, 997–1010.

Sobrino, J. A., & Raissouni, N. (2000). Toward remote sensing methods of land cover dynamic monitoring: Application to Morocco. *International Journal of Remote Sensing*, *21*, 353–366.

Stone, B., & Rodgers, M. O. (2001). Urban form and thermal efficiency: How the design of cities influences the urban heat island effect. *Journal of the American Planning Association*, *67*, 186–198.

Taha, H. (1997). Modeling impacts of increased urban vegetation on ozone air quality in the South Coast Air Basin. *Atmospheric Environment*, *30*, 3430–3432.

Ulrich, R. S. (1986). Human responses to vegetation and landscapes. *Landscape and Urban Planning*, *13*, 29–44.

Verstrate, M. M., & Pinty, B. (1996). Designing optimal spectral indexes for remote sensing applications. *IEEE Transactions in Geosciences and Remote Sensing*, *34*, 1254–1265.

Vitousek, P. M., Mooney, H. A., Lubchenco, J., & Melillo, J. M. (1997). Human domination of earth's ecosystems. *Science*, *277*, 494–499.

Voogt, J. A., & Oke, T. R. (1997). Complete urban surface temperatures. *Journal of Applied Meteorology*, *36*, 1117–1132.

Voogt, J. A., & Oke, T. R. (1998). Effects of urban geometry on remotely-sensed surface temperature. *International Journal of Remote Sensing*, *19*, 895–920.

Wellar, B. S., & Estes, J. E. (1968). On applications of aerial infrared imagery. *Annals of the Association of American Geographers*, *58*, 411–415.